



HAL
open science

Effect of magnetism on the atomic structure and properties of 5 grain boundaries in fcc Fe and fcc Ni

Abdelhay Zair, Myriam Sansa, Adnene Douhbi, Fabienne Ribeiro, Guy Treglia

► To cite this version:

Abdelhay Zair, Myriam Sansa, Adnene Douhbi, Fabienne Ribeiro, Guy Treglia. Effect of magnetism on the atomic structure and properties of 5 grain boundaries in fcc Fe and fcc Ni. *Acta Materialia*, 2022, 226, pp.117636. 10.1016/j.actamat.2022.117636 . hal-03647774

HAL Id: hal-03647774

<https://hal.science/hal-03647774>

Submitted on 20 Apr 2022

HAL is a multi-disciplinary open access archive for the deposit and dissemination of scientific research documents, whether they are published or not. The documents may come from teaching and research institutions in France or abroad, or from public or private research centers.

L'archive ouverte pluridisciplinaire **HAL**, est destinée au dépôt et à la diffusion de documents scientifiques de niveau recherche, publiés ou non, émanant des établissements d'enseignement et de recherche français ou étrangers, des laboratoires publics ou privés.

Effect of magnetism on the atomic structure and properties of $\Sigma 5$ grain boundaries in Fe and Ni

Abdelhay Zair^{1,2,3}, Myriam Sansa², Adnène Dhouib⁴, Fabienne Ribeiro⁵, and Guy Tréglia¹

¹*Aix Marseille Université, CNRS, CINAM (Centre Interdisciplinaire de Nanosciences de Marseille),*

Campus de Luminy, Case 913, 13288 Marseille Cedex 9, France

²*Universit de Tunis El Manar Thermal Radiation Research Unit, Faculty of Sciences of Tunis, El Manar 1, 2092 Tunis, Tunisia*

³*Universit de Carthage, Faculty of Sciences of Bizerte. Zarzouna Tunisia*

⁴*College of Sciences, Department of Chemistry,*

Imam Abdulrahman Bin Faisal University,

31113 Dammam City, Saudi Arabia and

⁵*IRSN (Institut de Radioprotection et de Sûreté Nucléaire),*

PSN-RES, SEMIA, LPTM, 13115 St Paul Lez Durance cedex, France

(Dated: August 18, 2021)

Abstract

Grain boundaries (GB) play a major role in the mechanical properties of steel. We model here the most common $\Sigma 5$ (210) and (310) [001] tilt boundaries in fcc Ni and Fe which are main components of steel, paying particular attention to the effect of magnetism on the relative stabilities of the competing GB structures and on their main characteristics (excess volume, microstructure, stress profile, ...). To this aim we develop a new interatomic potential in the second moment approximation of the Tight-Binding scheme which accounts for magnetism in order to relax the structures within quenched molecular dynamics simulations. Similar results are obtained for Fe and Ni, even though magnetic effects are found much more important in the former case. More precisely, magnetism significantly lowers the excess GB energy and volume, strongly reduces the stress in the GB region, and can even modify the microstructure in some cases. Finally a local analysis is proposed which allows to classify the relative stabilities of the different structures in terms of only a few given atomic sites.

I. INTRODUCTION

Grain boundaries (GB) represent one of the most important 2D defect which have been studied in material science due to their decisive influence on polycrystalline solids properties such as strength, electrical resistivity and corrosion [1] [2]. They can be viewed as a junction where two surfaces touch, the corresponding space being described by a set of five macroscopic degrees of freedom defining the relative rotation of the two neighboring grains and the orientation of boundary plane relative to the grain [3]. The dependency of the GB properties with this set of geometrical variables is not fully understood but some of GB related features seem to have more impact on the GB complex related phenomena [4]. Simple models can be used to illustrate the correlations between GB properties and macroscopic geometrical identification. Indeed, GB are associated with an excess volume, an additional free space compared to the bulk. Computational and experimental efforts have been used to rationalize the variation of GB energy with this volume expansion and the population of the GB. Wolf and Phillpot [5] observed that GB oriented perpendicular to close-packed directions have lower energies. Similarly to free surfaces, Wolf [6] proposed that this GB energy can be understood in terms of broken bonds for symmetric and asymmetric tilt and twist boundaries.

It is a challenge to detect and quantify experimentally GB excess volume but it has been studied in bi- and polycrystallines samples, in which case what is measured corresponds to an average over many GB types. Experimentally, results indicate that there is a higher population and therefore a lower energy for grains that terminate on low-index planes with large excess volume due to large interlayer spaces [7]. Read and Shockley [8] predicted the energy of a low-angle GB by a classic dislocation based model and Wolf demonstrated that the energy predicted by this approach can be extended to high-angle boundaries.

A good agreement between experiment and simulation proves that both approaches are reliable when carefully applied. Holm et al. [9] computed a large number of GB energies in FCC metals using EAM interatomic potentials and found convincing results. Yesilitem and Arias [10] showed, in the framework of Generalized Pseudopotential Theory, that the boundary energy of (110) symmetric tilt boundary in BCC molybdenum strongly depends on incorporated vacancies, going from 0.61 to 2.13 J/m^2 when half of the atoms in the plane adjacent to the GB are removed.

In addition to the geometry/energy relationships, a lot of interest is given to boundary property dependency with microstructure and chemical composition. High resolution transmission electron microscopy has been used to probe the GB structure down to the atomic level. The studies of segregation elements to GB and their modified diffusion [11] confirm the importance of microstructure from an energetic point of view. These results are consistent with different simulation works. Ratanaphan et al. [12] reported minimized energy of several identical GB with different microscopic starting states and noted that there is no guarantee that a global minimum energy is always reached. Berthier et al. [13] showed that the relative stabilities of microstructures depend on the used potential and proved that phase transition between multiple patterns can be driven by temperature.

Magnetism is in general not included in theoretical investigations in spite of the growing interest of scientific in iron and nickel GB due to their industrial uses. Most first principal studies performed in this context concerned the variation of the magnetic moment in the GB region. Thus Hampel et al. [14] studied $\Sigma 5(310)$ symmetrical tilt GB in iron, using KKR method and reported the enhancement of the magnetic moment at the GB ($2.56 \mu_B$) compared to its bulk value ($2.35 \mu_B$). Geng et al. [15] found similar results concerning the $\Sigma 5(210)$ GB in nickel, where the magnetic moment is slightly enhanced at the GB ($0.67 \mu_B$) with respect to its bulk value of $0.6 \mu_B$. Still in bcc iron, Bhattacharya et al. [17] found that the magnetic moment varied locally with the environment of atoms in the vicinity of $\Sigma 3(111)$ and $\Sigma 11(332)$ GBs and that this modifies the stress undergone in this region. Even though less studies of the effect of magnetism on GBs exist for fcc iron, one can mention somewhat similar *ab initio* studies in the case of stacking fault energies. Thus Bleskov et al. [16] showed that magnetism is essential to stabilize austenitic structure in iron and reduces the energetic barrier to overcome to form the intrinsic stacking fault.

All these results confirm that coupling magnetism and microstructure might be important.

Even though progress in *ab initio* calculations have made them well suited tools to analyse GB structure, there is still need of simpler energetic models to study kinetics processes involving GB, in particular when magnetism plays a role, as it is the case for steel aging. In this context, the present work is an attempt to investigate $\Sigma 5$ GB in FCC iron and nickel, as representative of high angle high energy GB, using interatomic potentials derived to this aim within the second moment approximation of the Tight-Binding scheme (TB-SMA).

It is worth pointing out that our aim here is not to study the possible variation of magnetic characteristics, such as magnetization or Curie temperature, in the grain boundary region, but instead to treat in an effective way the effect of magnetism on the energy interactions, in order to identify how magnetism can modify the main characteristics (microstructure, stress profile) close to the grain boundary

Even though FCC Fe is metastable at 0 K, the Fe-Ni phase diagram presents an austenitic FCC γ phase which extends from pure FCC Fe to pure FCC Ni at the temperature of use for industrial (*e.g.* nuclear) applications. Indeed nickel is a γ stabilizer in iron, so that a preliminary study of FCC iron is a necessary step to a future investigation of austenitic Fe-Ni steel properties in both dilute limits. We first present the methodology used, paying particular attention to the derivation of a TB-SMA potential able to differentiate magnetic and non magnetic state. We then present the main global results (formation excess energy, excess volume) obtained for the different GB configurations and magnetic states, before presenting a more local view (microstructure, energy and pressure maps) of the GB region. Finally, we propose a local analysis of the relative stabilities of the different GB structures based on the later results.

II. METHODS

A. GB structures generation

The macroscopic structure of GB is characterized within the *CSL* model [18], in which case it is labelled as $\Sigma(hkl)[mno]$ where Σ is the reciprocal density of coincidence sites in the lattice. Each macroscopic orientation is described by the tilt axis $[mno]$ (*z-direction*) and the crystallographic plane of the GB (hkl) (*x-direction, y-direction*) and labelled as $\Sigma(hkl)[mno]$. Among all the grain boundaries in fcc metals, the most studied are the $\Sigma 5(h10)[001]$ tilt boundaries for $h = 2, 3$. These are the orientations that will be studied here in FCC nickel and iron. These tilt boundaries are obtained by rotating two FCC grains around the $[001]$ axes by a given angle α ($\alpha = 53.13^\circ$ for $h = 2$, $\alpha = 36.87^\circ$ for $h = 3$). Periodic conditions are then applied in the three directions, so that we obtain two equivalent reversely oriented GB in the simulation box. We ensure that the distance L_x between the generated GB is sufficiently large to neglect any elastic interaction between them. For instance, in the case

of Fe $\Sigma 5(210)$ the dimensions of the simulation box are $L_x=48.24 \text{ \AA}$, $L_y=23.88 \text{ \AA}$, $L_z=10.68 \text{ \AA}$, with a lattice parameter of 3.56 \AA .

In the case of $\Sigma 5(210)[001]$, the rotation of the two FCC grains leads to the *CSL* positions of the structure labelled B'.B' (Figure 1), using the nomenclature of structural units [19]. However, according to the same authors, an other structure labelled B.B can be obtained from B'.B' by adding a shear of $[1-20]a/10$, where a is the lattice parameter (see Figure 1). These two structures have been shown to compete depending on the element under consideration, and on the interatomic potential used in the simulations. We will then study both here for Fe and Ni.

In the case of $\Sigma 5(310)[001]$, the rotation leads to the structure shown on the righthand side of the Figure 2. However, as can be seen, two atoms per unit cell are found very close (precisely closer than 0.3 \AA) to one another on each part of the boundary. This led some authors to mix these dimers into a single monomer, to form the so-called *C* structure which is shown in the left part of the Figure 2, and presented as the stablest one in general. However, we will also consider here the initial structure with dimers, that we will label C_0 .

In order to determine the ground state of a $\Sigma(hkl)[mno]$ GB, we perform a total energy minimization starting from the ideal structures mentioned above. In addition, in the case of $\Sigma 5(210)[001]$, we construct a set of metastable configurations with different microscopic structures using a $\delta - surface$ approach [20] [21]. Herein, the two grains of a GB are shifted with respect to each other, in the (y,z) -plane parallel to the GB, with a spacing of fifth the cell length a . Following these translations, once again if any two atoms are closer than 0.3 \AA , one is deleted to obtain a more realistic configuration. The ground state corresponds to the state of lower energy (between all relaxed microstructures in a set).

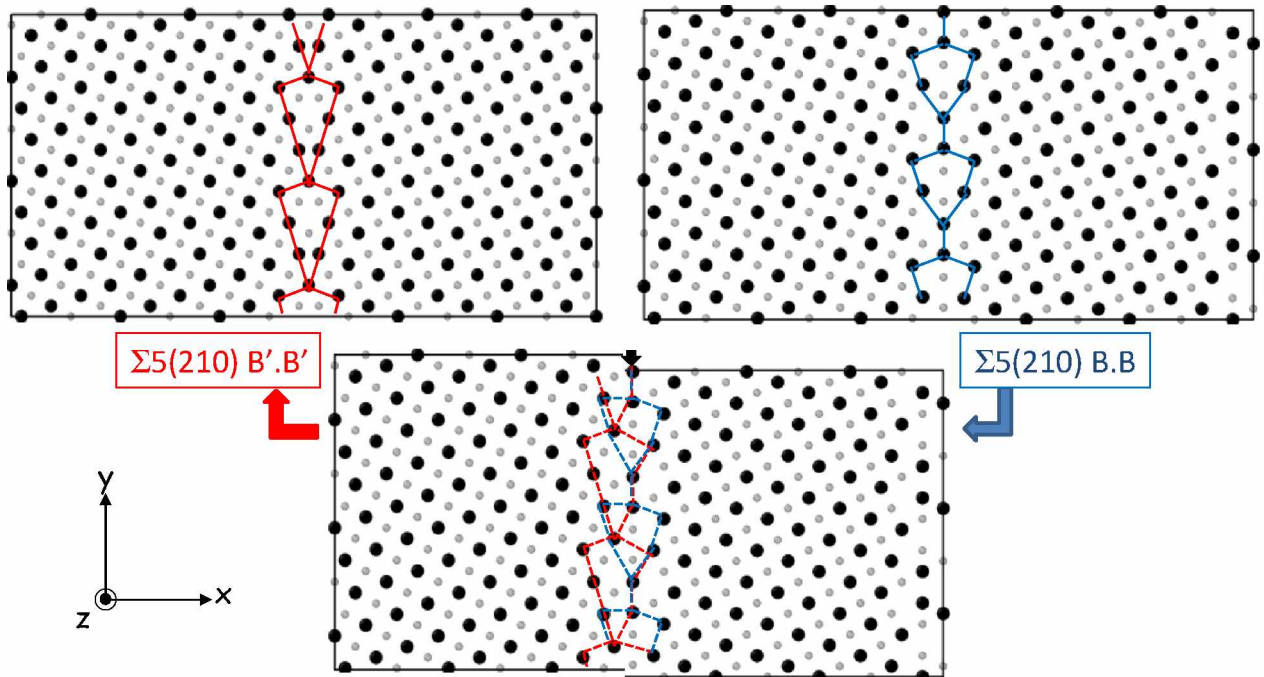


FIG. 1: Projection along the tilt axis of the two ideal B'.B' and B.B microstructures encountered in the $\Sigma 5(210)[001]$ GB. A different grey level is used for each (001) plane along the (z -direction). The B'.B' and B.B units contained in one period of the boundary are indicated in full lines. The lower figure represents the transition state from the later to the former.

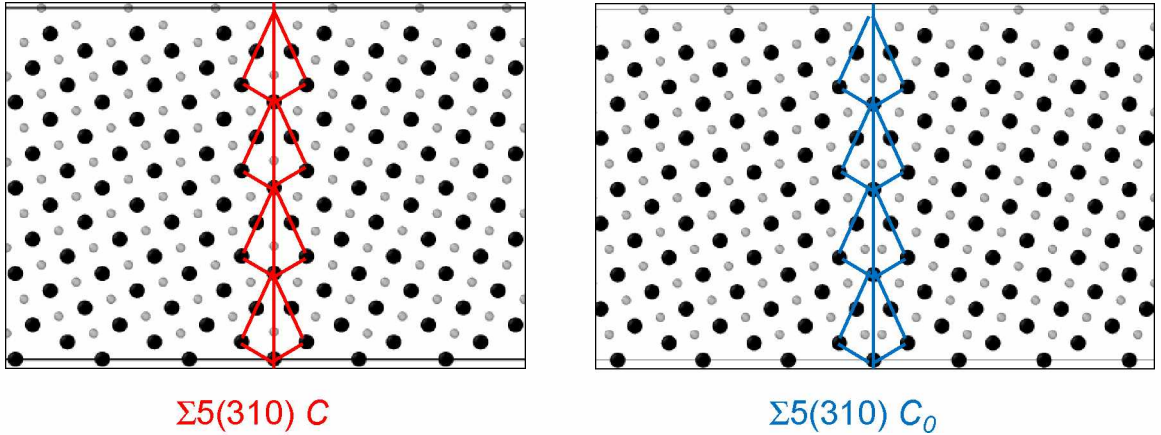


FIG. 2: Projection along the tilt axis of the two ideal C and C_0 microstructures encountered in the $\Sigma 5(310)[001]$ GB. A different grey level is used for each (001) plane along the (z -direction). The C and C_0 units contained in one period of the boundary are indicated in full lines.

B. SMA potential for non magnetic and ferromagnetic Fe and Ni elements

Modeling Fe and Ni GB through atomistic numerical simulations requires to get an interatomic potential sufficiently simple (analytical) to be not too much computational time consuming, and in the same time sufficiently reliable to ensure to save the essential physics, and in particular the possible effect of magnetism. The second moment approximation of the Tight-Binding formalism (TB-SMA [22]) is particularly well suited to this aim **in the case of close-packed structures such as the fcc one considered here**. The cohesive energy in this approximation writes:

$$E_{coh} = -\beta \sqrt{\sum_r \exp^{-2q(\frac{r}{r_0}-1)}} + A \sum_r \exp^{-p(\frac{r}{r_0}-1)} \quad (1)$$

where r_0 is the distance between first neighbors in equilibrium bulk and the summation is performed up to second neighbors. As usual, the curve is then smoothly truncated between second and third neighbors, respectively at cut-off distances r_c^1 and $(r_c^2$, through a 5th order polynomial termination. The knowledge of the potential then requires to determine the four parameters (p , q , A , β) for each element, in both the non magnetic and ferromagnetic cases. This is performed here by fitting the universal state equation of Rose [23], which links values of dimensionless energies and distances scaled with respect to the respective values of the

cohesive energy, lattice parameter and bulk modulus for each element under consideration.

Let us remind that we study here both Fe and Ni in the fcc structure. We then need to determine the latter values for both elements in this structure, in both the non magnetic and ferromagnetic states, which is achieved by performing the corresponding DFT calculations, using the VASP code in the GGA approximation (PBE functional) which are then rescaled to the experimental values of the cohesive energies. In the ferromagnetic state, the magnetic moment μ is optimized for each distance. The resulting values are shown as dots and squares in Figure 3 for both Fe (left) and Ni (right). The most striking feature is the unusual behaviour observed for the Fe curve in the ferromagnetic case, which presents a very flat minimum. A closer view (see left-hand-side of Figure 4) reveals that this behaviour is due to the existence of two different minima as a function of the interatomic distance. Looking at the corresponding variation of the magnetic moment, exhibited on the right-hand-side of Figure 4 reveals that these two minima are associated to two different values of the magnetic moment, which presents an abrupt transition with increasing distance (corresponding to low and high magnetization respectively), consistently with the results in the literature [24].

The question is then how to account of this magnetic transition in the framework of the simple TB-SMA interatomic potential (equation 1). Several alternatives exist depending on that one needs to treat it explicitly or not. In the former case, many ways exist to treat explicitly magnetism in the Tight-Binding formalism, by an appropriate coupled self-consistent treatment of both electronic charge and spin allowing to determine both the magnetic energy and the magnetic moment [25–28]. In the later case, if one is mainly interested by treating implicitly the effect of magnetism on the energy calculation, a two-band TB-SMA model has been proposed by Ackland [29] in presence of two different spin-subbands. In the same spirit, one could treat implicitly the present magnetic transition by combining two different SMA potentials fitted to the two DFT curves obtained by fixing one or the other magnetic moment (see right-hand-side of Figure 4). Here we chose a still simpler manner to treat implicitly this magnetic transition by assuming that its main effect on the variation of energy with distance is its effective flatness around the two minima (or equivalently the corresponding low value of the effective bulk modulus) and then fit a single SMA potential in order not to lose its simplicity. The so fitted SMA parameters p , q , A , β are given in Table I in which are also given the calculated values of essential physical quantities such as the cohesive energies, lattice parameters, bulk modulus, elastic constants, which are

compared to their experimental counterparts. The corresponding TB-SMA energy curves are compared to the DFT ones in Figure 3, revealing a quite good agreement. Let us point out that this way to treat implicitly, in an effective way, magnetism in the SMA formalism is fully consistent with its original derivation, which implicitly accounts of the electronic structure while losing its detailed description.

Before going further, let us recall that the present SMA potential has been fitted to model the fcc crystalline structure of both Ni and Fe. Indeed, whether SMA is fully justified for close-packed structures only, such as fcc or hcp, it is less for more open ones such as bcc which would require going beyond second moment approximation, even though this is sometimes bypassed by playing on the cut-off radius at the price of losing its electronic structure grounds. This means that the potential defined should not be suited to study the bcc Fe structure. This is illustrated in Figure 3 in which we have nevertheless added the corresponding curves for bcc Fe in both magnetic states. Indeed even though the overall distance behavior not so bad reproduce the respective stabilities of ferromagnetic and non magnetic structures and in particular the variation of the equilibrium distance of the NM and FM states, it strongly underestimates the magnetic energy gain around these equilibrium distances. This potential will then only be used and extended to study the effect of magnetism on austenitic FeNi steels.

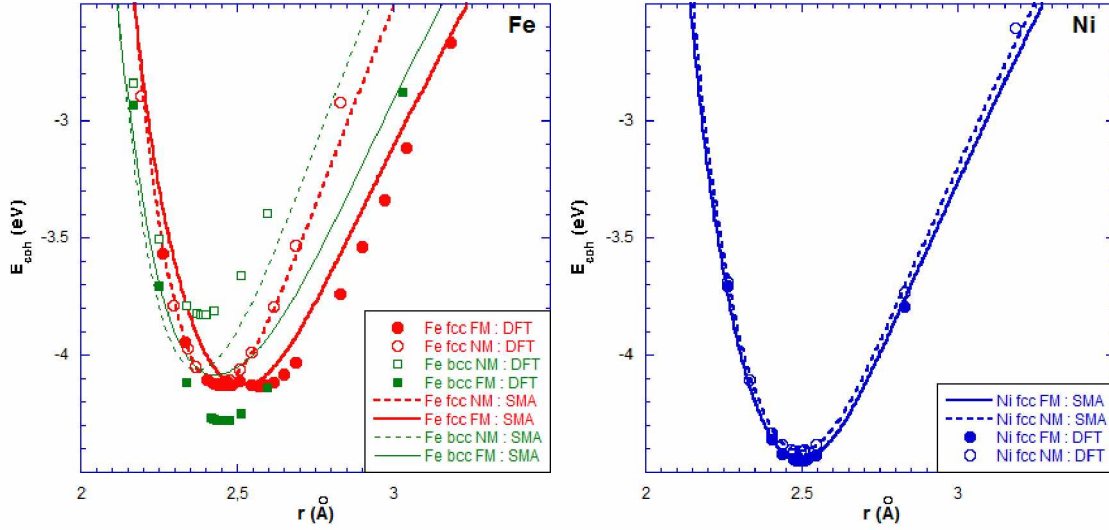


FIG. 3: Variation of the cohesive energy as a function of the interatomic distance from DFT calculations for Fe (left-hand-side) and Ni (right-hand side) in the non magnetic (empty dots and squares) and ferromagnetic (full dots and squares) states. The calculations have been performed in both the fcc (red symbols) and bcc (green symbols) structures for Fe but only in the fcc one (blue symbols) for Ni. The corresponding TB-SMA curves are given in dotted lines for the non magnetic state and in full lines for the ferromagnetic one.

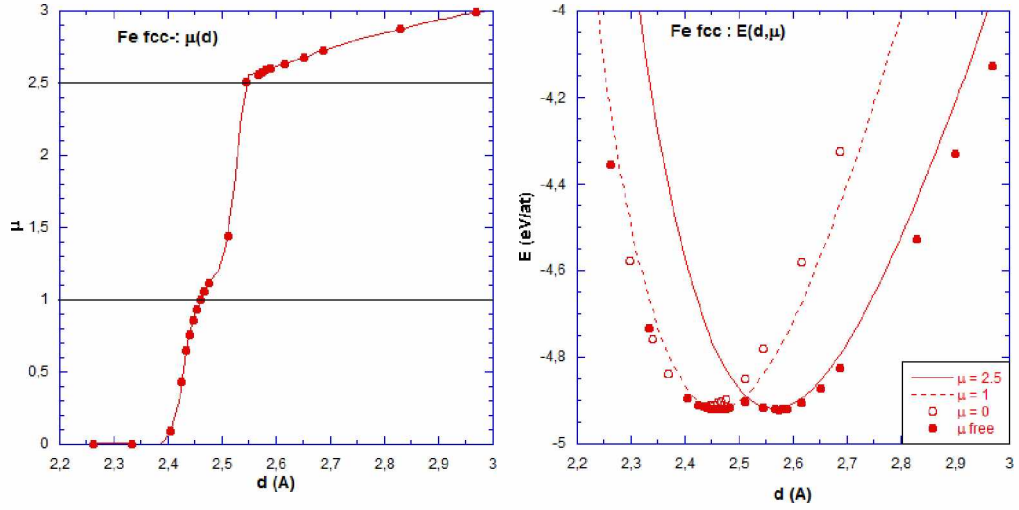


FIG. 4: Left-hand-side: variation of the magnetic moment as a function of distance from DFT calculations in which μ is not fixed for fcc Fe. Right-hand-side: zoom of the energy curves of Figure 3 around the minimum for fcc Fe, in the non magnetic (empty dots) and ferromagnetic (full dots) states. The full and dotted curves correspond to DFT calculations performed for two fixed magnetic moments ($\mu=1 \mu_B$ and $\mu=2.5 \mu_B$).

	Fe-Fe (FCC)		Ni-Ni (FCC)	
	NM	FM	NM	FM
p	10.76	8.64	8.96	8.76
q	3.58	2.88	3	2.92
$A(eV)$	0.1724	0.1729	0.1860	0.1863
$\beta(eV)$	1.7682	1.7596	1.8866	1.8969
$r_0(\text{\AA})$	2.44	2.52	2.50	2.50
$E_{coh}(eV)$	- 4.12	- 4.13	- 4.41	- 4.45 (- 4.45)
$B(10^{12}ergs/cm^3)$	2.78 (2.81)	1.66 (1.67)	1.95 (1.97)	1.88 (1.89)
$C_{44}(10^{12}ergs/cm^3)$	1.11 (1.16)	0.67 (1.16)	0.79	0.76 (1.32)
$C'(10^{12}ergs/cm^3)$	0.4	0.21	0.25	0.24 (0.55)

TABLE I: TB-SMA parameters and calculated values of the cohesive energies, bulk modulus, elastic constant, compared to their experimental counterparts (in parenthesis). The lattice parameter a is given by : $a = r_0\sqrt{2}$.

III. LOOKING FOR THE STABLEST MICROSTRUCTURES

A. Energy

1. Excess GB formation energy

All calculations were done within the TB-SMA potentials presented above. The total energy was minimized using a quenched molecular dynamics method (QMD). Periodic conditions were performed in three directions and the total energy was minimized with respect to atomic positions (x_i, y_i, z_i) and the one dimension L_x of the simulation box perpendicular to the grain boundary direction, *i.e.* the x -direction.

As mentioned previously, for the (210) orientation, two initial conditions were used corresponding to ideal B'.B' and B.B, together with a set of shifted configurations, whereas only the two ideal C and C_0 were used for the (310) orientation. In the former case, it is worth noticing that whatever the initial configuration, even starting from the B.B one, all simulations lead to the B'.B' final configuration. Such an easy deformation can be understood from the double gliding mechanism which allows to go from one to the other illustrated in Figure 1. The only way to keep the B.B configuration is to fix the GB coincidence layer in order to avoid the gliding. Anyway, this means that in that (210) case the B'.B' configuration is the stable one. No such transformation occurs for (310), which implies to look at the GB formation energies to determine the stablest structure. These formation energies E_{GB} , also called excess energies, are defined as:

$$E_{GB} = \frac{E_{tot} - NE_{coh}}{2A} \quad (2)$$

where E_{tot} is the optimized total energy, N is the number of atom, E_{coh} is the bulk cohesive energy and A is the cross section area of the simulation cell ($A = L_y L_z$). We report the formation energies of the ground states in Figure 5.

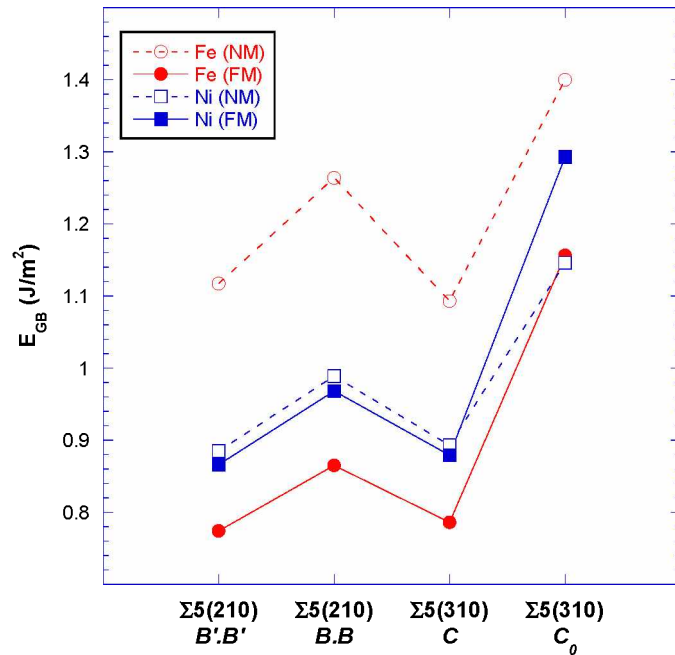


FIG. 5: Variation of the grain boundary energy (in J/m^2) for the four GB and the two magnetic states of Fe and Ni.

As can be seen, the B'.B' microstructure is indeed found to be the stablest microstructure for the (210) orientation while C is the one for the (310) GB, whatever the nature of the element (Fe, Ni) and the magnetic state. However, although magnetism plays almost no role on the value of the energy for Ni, it significantly decreases it (30 % reduction) in the case of Fe. As a consequence the Fe GB energies are higher than Ni ones in absence of magnetism, and lower when it is present. In other words, it is easier to form a GB defect for Ni than for non magnetic Fe but more difficult than for ferromagnetic Fe. It can be noticed also that the values of (210) and (310) energies are almost similar in the stablest (B'.B' and C) configuration, whatever the element and the magnetic state, although they differ for the B.B and C_0 ones. These values are consistent with those resulting from EAM calculations for non magnetic BCC iron (1.11 J/m² [12]), but somewhat lower for FCC nickel (1.23 J/m² [30]). Finally let us recall that the present stabilities are determined at T=0K, and that the small differences found between the different structures, in particular between B'.B' and B.B, suggest that the stablest ones could be reversed at finite temperature due to entropic effects.

2. Separation work and fracture

a. Separation work: To quantify the GB stability, we compute the separation work W_{sep} which is the work needed to separate reversibly two grains [31]. This is an important parameter in fracture mechanics, which is defined as:

$$W_{sep} = 2E_{FS} - E_{GB} \quad (3)$$

where E_{FS} is the energy of the free surfaces formed by separating the two grains. To determine this quantity, we relax a semi-infinite simulation box in which we suppress the boundary condition perpendicularly to the GB, *i.e.* along the x-direction. The system is then composed by a GB and two free surfaces as illustrated in Figure 6. The surface energies E_{FS} of the (310) and (210) relaxed surfaces are given in Table II.

	Fe		Ni	
	NM	FM	NM	FM
E_{210}	1.33	1.25	1.35	1.37
E_{310}	1.51	1.42	1.53	1.55
γ^{PCP}	1.95	1.95	2.2	2.2

TABLE II: Calculated values of relaxed (210) and (310) surface energies E_{FS} and experimental one for the usual cleavage plane γ^{PCP} . Units are J/m^2 .

This separation work determines how much the GB is stable compared to the corresponding free surface. Its variation with the nature of the element, its magnetic state and the structure of the GB, is displayed in Figure 6. In each cases, the value of W_{sep} is found larger for the magnetic configuration, contrary to what occurs for the excess energy, the effect being once again much more noticeable for iron. This separation work is higher for Ni than for Fe, and for the (310) GB than for the (210) one. Let us note that, as expected, the values of the separation work are larger for the stable B'.B' and C structures which are more difficult to separate than the others.

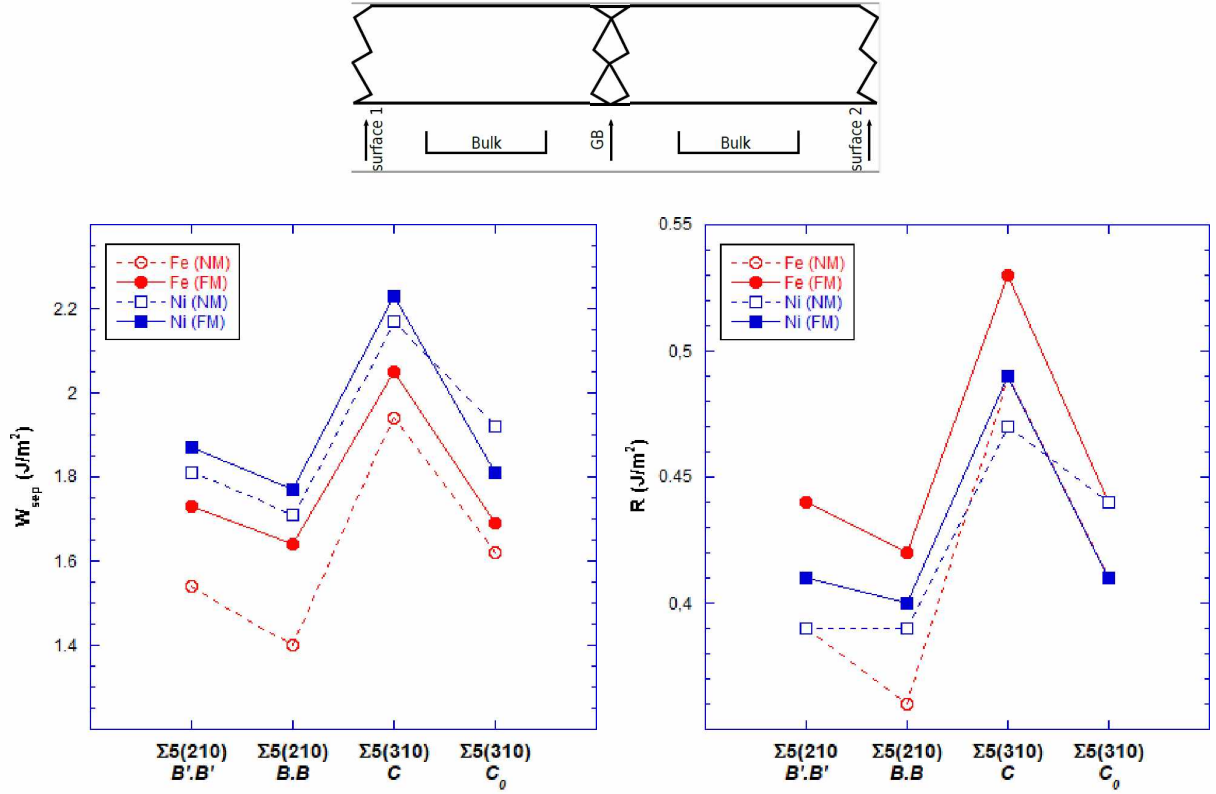


FIG. 6: **upper side**: simulation box: the distances between the GB and the surfaces must be large enough to neglect any elastic interactions and obtain bulk properties between the defaults. **lower side**: separation work (*left*) and R factor (*right*)

b. Intergranular/transgranular fracture parameter Cleavage fracture can be defined as rapid propagation of a crack along a particular crystallographic plane. The preferred cleavage planes are those with the lowest packing density. In the case of BCC crystal there exists a ductile/brittle transition temperature below which the material is brittle and breaks by cleavage on (100) or (110) planes. FCC metals normally do not cleave, because there are ample slip systems (corresponding to a close packed planes/directions) for ductile behavior at all temperature. However, some FCC metals may cleave under certain circumstances (for example austenitic stainless steels in stress-corrosion cracking conditions [32]). In the brittle regime, some metals break by cleavage through the grain (transgranular fracture), while others break by crack propagation along GB (intergranular fracture). The preference for either intergranular or transgranular fracture can be evaluated by the ratio R defined as:

$$R = W_{sep}/2\gamma^{PCP} \quad (4)$$

where γ^{PCP} is the surface energy of the preferred cleavage plane, given in Table II

If R is close to unity, transgranular cleavage is preferred, while for lower values intergranular fracture is expected [20]. We report the different values of R corresponding to each studied system in Figure 6. As can be seen, the overall trend followed by R is similar to that followed by W_{sep} , with values around 0.5 which indicates a preference for intergranular fracture whatever the situation. However a few differences are found since the R curves for Ni are found in-between those for FM and NM Fe whereas the W_{sep} ones were higher than both. The impact of magnetism is therefore stronger on R than on W_{sep} for Fe, leading to a more marked preference for intergranular fracture for Fe than for Ni in the FM case whereas the reversed effect is observed in the NM case.

B. Global deformation

1. Excess GB volume

Let us first perform a global analysis of the GB structure. It is usually characterized by its excess volume per unit area of the boundary, related to the mismatch in grain lattices, which plays an important role in the stability of the GB. It is defined as:

$$\delta V = \frac{V_{tot} - V_0}{2A} \quad (5)$$

where V_{tot} is the volume of the relaxed simulation cell containing N atoms and including two GB, and V_0 is the corresponding perfect bulk volume, defined as $V_0 = Na^3/4$. From this definition, one can define the dimensionless excess volume per unit area of the boundary in units of the lattice constant:

$$\frac{\delta V}{a} = \frac{L_x}{2a} - \frac{N}{8} \frac{a^2}{L_y L_z} \quad (6)$$

If $\delta V/a$ is negative (resp. positive) then the GB region contracts (expands) and its absolute value characterizes the magnitude of the deformation. One can see in the left part of Figure 7 that, whatever the nature of the element, of the magnetic state and of the GB under consideration, the GB region extends, leading to a positive excess volume. If one now

looks in more details, one finds however differences between the different cases. The most striking feature is the drastic impact of magnetism for Fe for which it decreases the excess volume by about a factor two whereas it plays no role for Ni. It can be also noted that, except for the B'.B' structure, the curves are similar for Ni and non magnetic Fe.

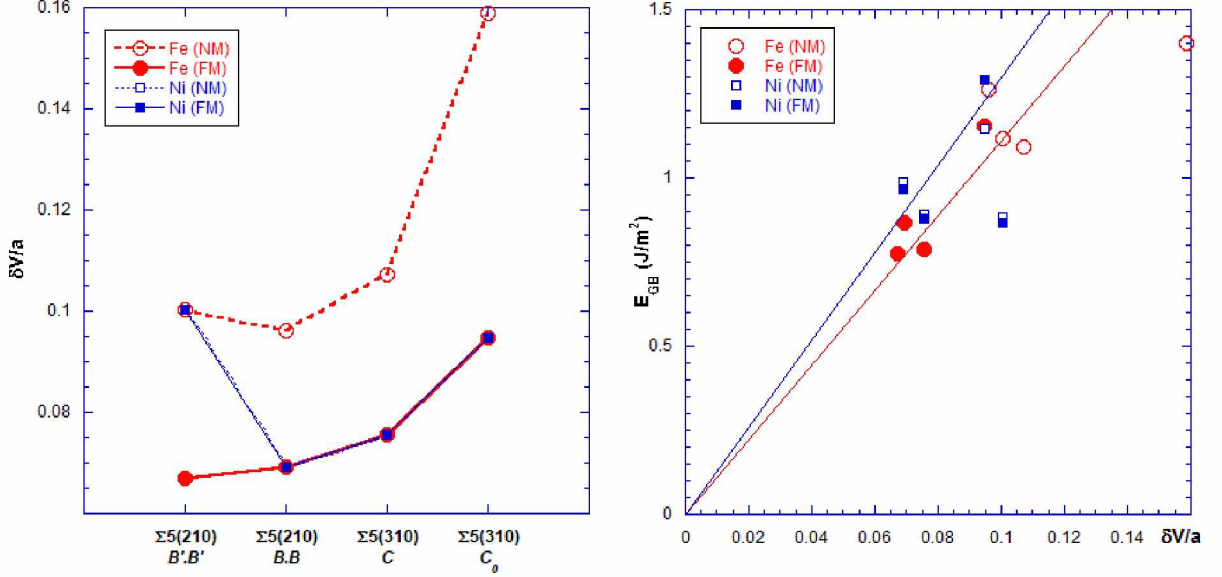


FIG. 7: (*left*) Variation of the excess volume per unit area ($\delta V/a$) with GB orientation for the four GB and the two magnetic states of Fe and Ni. (*right*) Correlation between the excess GB energy and this excess volume. The blue line is the linear law derived from references [30, 33] for Ni. The red one is the linear relationship fitted from the present calculations for Fe.

One can wonder how the excess grain boundary energy varies with the net expansion of the grain boundary. To answer this question, previous studies using EAM potentials [30, 33] have been performed in the cases of Ni and Cu. Their results revealed a rough correlation between formation energy and excess volume per unit area for both metals, the overall trend being an increasing energy with increasing boundary expansion. More precisely they found roughly a linear correlation $E_{GB} \simeq \alpha \delta V/a$, which becomes more pronounced in the low formation energy limit. The coefficient of this relationship depends on the element under consideration, being almost twice larger for Ni than for Cu: $\alpha \simeq 13$ (8) for Ni (Cu). In order to check the generality of this correlation, we plot in the right part of Figure 7 the variation of E_{GB} (taken from Figure 5) as a function of $\delta V/a$ for both Ni and Fe metals. As can be

seen for Ni, our points are in overall good agreement with the previous linear relationship, except for the $\Sigma 5(210)[001]$ B'.B' structure which falls rather far away, showing the limits of the previous conjecture according to which the smallest the excess energy is the smallest the net expansion. For Fe, we find that the linear law is roughly obeyed whatever the magnetic state, with an intermediate slope between Ni and Cu, namely $\alpha \simeq 11$.

2. Microstructure

To go beyond the above global description, we now present in more details the local microstructure in the GB vicinity. This is done not only for the stablest structures, but also for the other ones which could be either stabilized at finite temperature in view of the small energy differences involved, or could appear as transition states during dynamic processes. In addition this local analysis will also help us to understand what are the elements which govern the stabilization of one or another structure.

a. $\Sigma 5(210)[001]$ GB : Let us first present in Figure 8 the two B'.B' and B.B microstructures obtained for (210) GB in the case of iron after relaxation. The first information given by the figure is that the GB microstructure does not depend on the magnetic state of the system, and that it is symmetrical in all cases. In addition, it can be seen that the microstructure close to the coincidence plane is more perturbed (broken line of the cell units) in the case of B'.B' than of B.B.

The corresponding structures for Nickel are shown in Figure 9. One recovers the main results of Fe, namely a symmetrical configuration which does not depend on the magnetic state. The main difference between the two elements is observed for the B'.B' GB for which the microstructure is less perturbed in the GB region for Ni than previously for Fe.

b. $\Sigma 5(310)[001]$: The results for the (310) GB are first shown for Fe in Figure 10. The configuration obtained for C is slightly asymmetric, magnetism playing almost no role on the structure. The situation is very different for C_0 which is found strongly perturbed and non symmetric in absence of magnetism, whereas introduction of magnetism symmetrises the structure. Note that in the later case, the GB layer has been shifted during the simulation. Let us also mention that, in both magnetic states, relaxation allows to avoid the too short interatomic distances initially present in the ideal C_0 (Figure 2).

As can be seen in Figure 11, a similar effect of magnetism is found in the case of Ni.

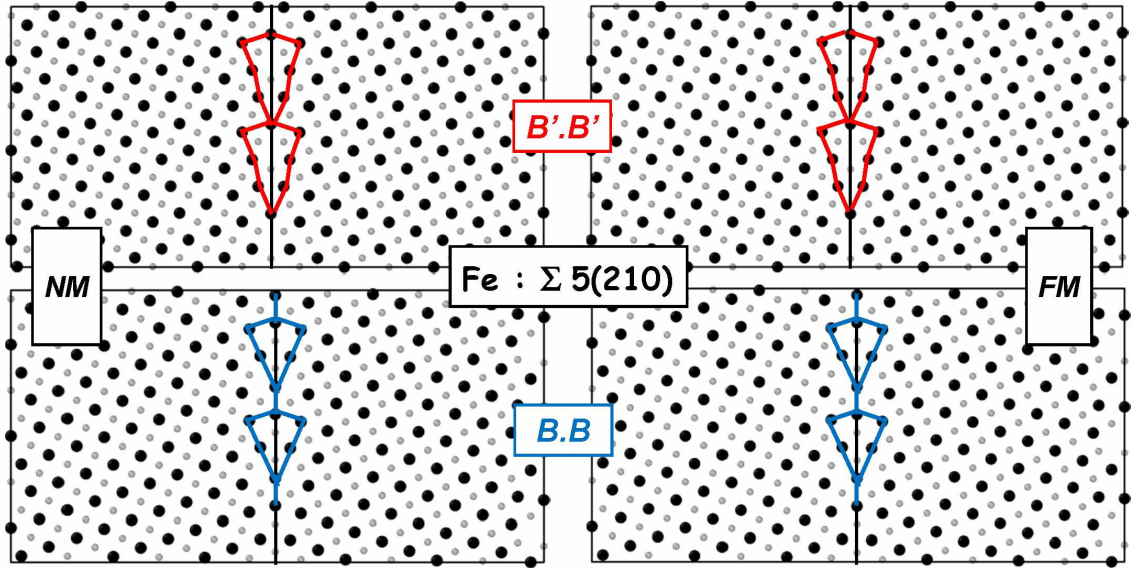


FIG. 8: Relaxed (210) $B'.B'$ and $B.B$ microstructures for Fe, in both magnetic states.

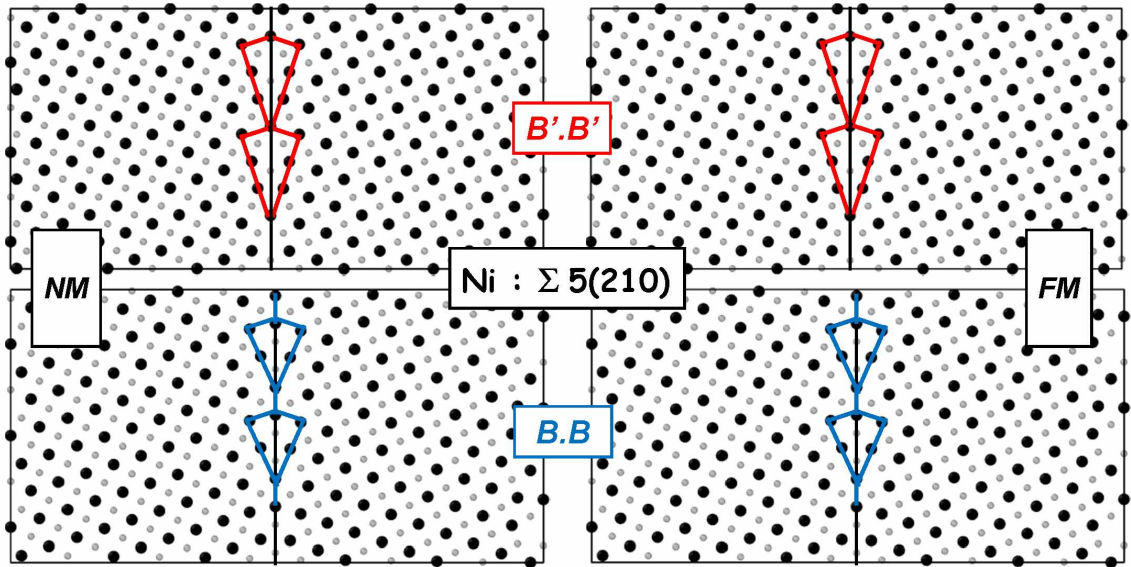


FIG. 9: Relaxed (210) $B'.B'$ and $B.B$ microstructures for Ni, in both magnetic states.

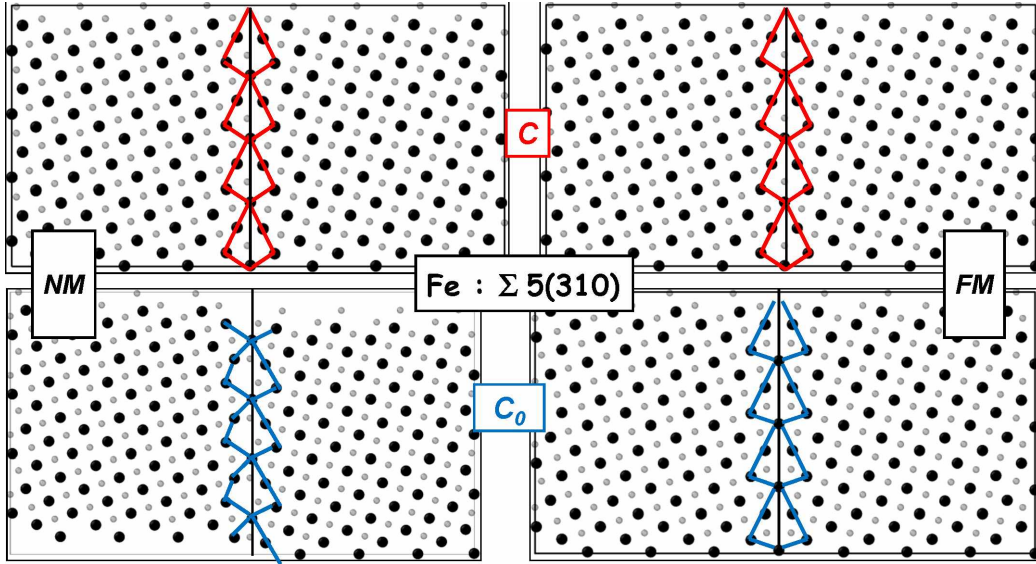


FIG. 10: Relaxed (310) C' and C_0 microstructures for Fe, in both magnetic states.

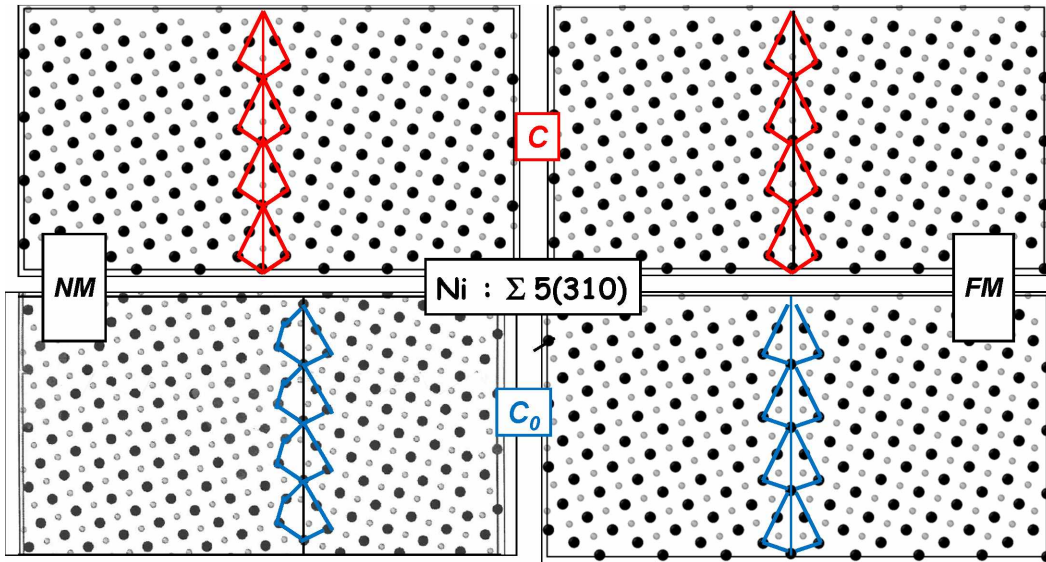


FIG. 11: Relaxed (310) C' and C_0 microstructures for Ni, in both magnetic states.

3. Profile and symmetry

In order to get a more detailed description of the microstructure and of the effect of magnetism on it, one can look at the distribution of distances between layers perpendicular to [001] planes. The planes perpendicular to the grain boundary in the fourth cases are labelled n , n taking integer or half-integers values as defined in Figure 12.

In the case of the (210) GB, one can see that the atoms belong to two [001] different planes. We note $n = 0$ the median layer containing two unequal atoms on the two unequal planes (top and low plane), $n = 1$ is the next layer which contains 2 unequal atoms on the two unequal planes and so on. The bulk interlayer distance for this orientation d_n between layers n and $n + 1$ is $d_{bulk} = 0.772 \text{ \AA}$ (resp. 0.792 \AA) for Fe (resp. for Ni).

For the (310) GB, the atoms belong to the two unequal [001] planes do not belong to the same vertical layer and define different interlayers. When n is even (resp. odd), the interlayer is formed by atom belonging to the so-called *top* (resp. *low*) planes. In that case d_n is the distance between the interlayers n and $n - 0.5$ except for $n = 1$ where d_1 corresponds to the distance between $n = 0$ and 1. This exception is due to a structural defect that is the absence of atoms in $n = 0.5$ or -0.5 . We have only one of these two types of atoms remaining in the structure. As one can see in Figure 12, we choose to characterize the ± 0.5 remaining type atom by the algebraic measure Δ from $n = 0$. Δ is positive (resp. negative) when the excess atom is to the right (resp. left) of $n = 0$. In fact one can consider the GB layer as a bilayer with thickness Δ . The bulk interlayer distance for this orientation d_n between layers n and $n - 0.5$ is $d_{bulk} = 0.546 \text{ \AA}$ (resp. 0.558 \AA) for Fe (resp. for Ni).

The situation being more complex for iron (magnetic differences, no mirror effect ...) than for nickel, it will be more detailed to present the notations and define the quantities used.

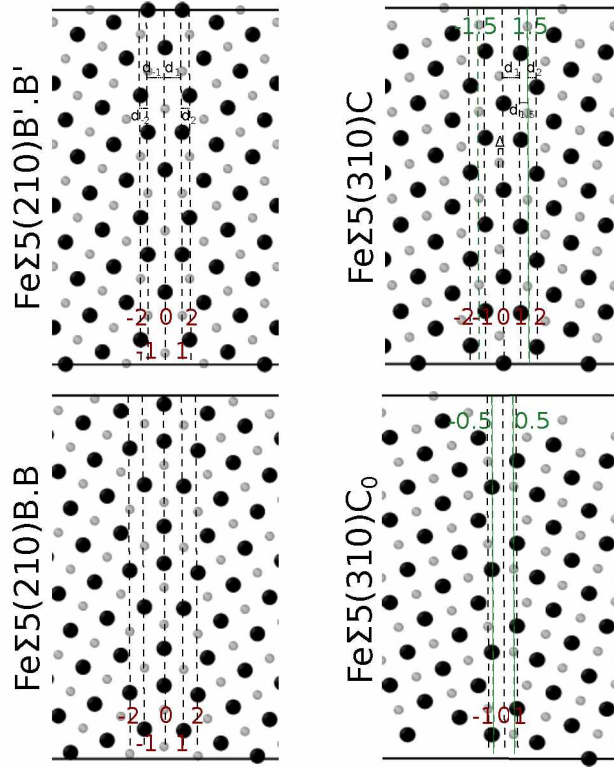


FIG. 12: Notation used to define the $\Sigma 5(210)[001]$ and $\Sigma 5(310)[001]$ interlayer distance profile for B'.B', B.B, C and C_0 GB structures. The grey and black atoms belong to two unequal planes (called top and low planes) perpendicular to the tilt direction [001].

a. $\Sigma 5(210)[001]$ iron interlayers configurations: Let us first comment on the distance profile obtained for the stable B'.B' structure. In Figure 13, we plot d_n/d_{bulk} as a function of n for the $\Sigma 5(210)[001]$ NM and FM configurations, d_{bulk} being the value reached by d_n in the bulk. Note that in this case, the profile is symmetrical so that $d_n = d_{-n}$. It is oscillatory in the GB region before being rapidly damped in the bulk (for $n > 5$). If we note u (resp. d) an interlayer distance such as $d_n/d_{bulk} > 1$ (resp. < 1), one can see that the oscillation does not follow a usual $\{...-d-u-d-u-...\}$ sequence but, for instance on the right of the GB layer, a more complex $\{u-d-u-u-d-0-0-...\}$ one (where 0 means no variation respective to bulk). The extension of the profile is of about 4 Å on each side of the GB layer.

In the case of the B.B structure, the profile is essentially the same, oscillating on about 4 Å on each side of the GB layer. The main difference is that this profile is more abrupt on each side with a larger dilation undergone by the first underlayer followed by weaker deformation on the other layers.

For both structures, one does not observe a significant influence of magnetism on the profiles.

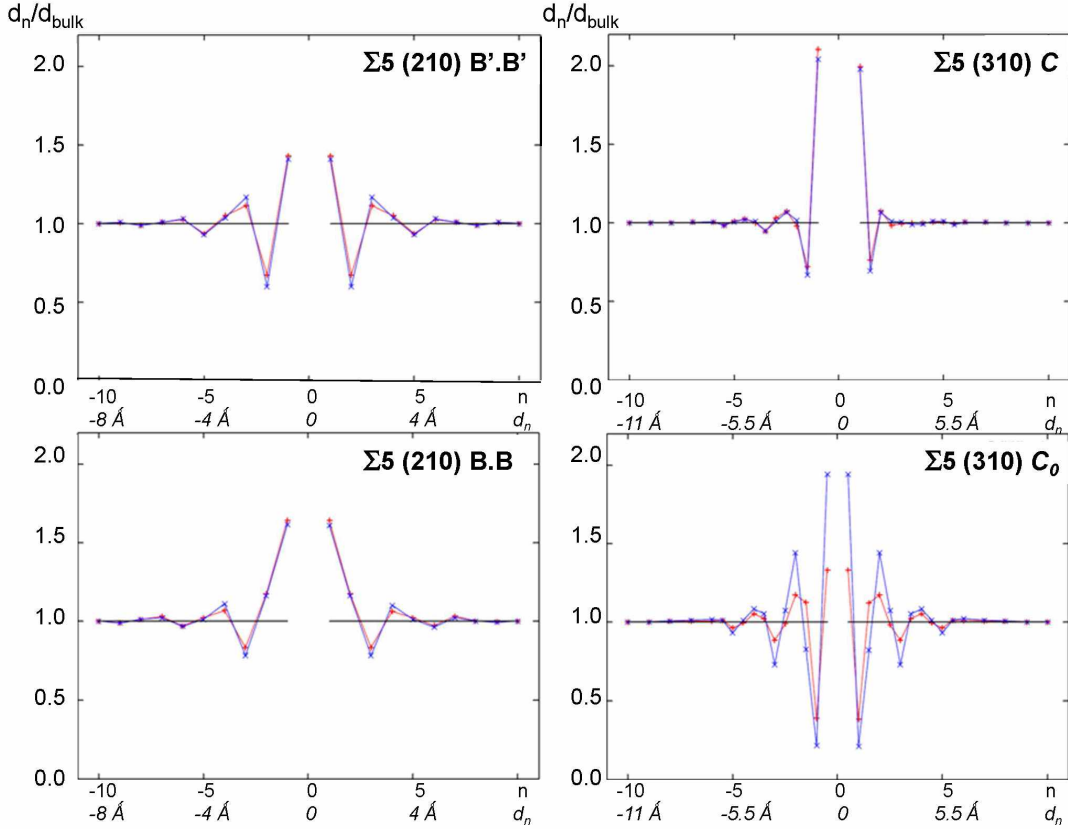


FIG. 13: Interlayer distance profiles d_n/d_{bulk} in both non magnetic (red line) and ferromagnetic (blue line) Fe for the $\Sigma 5(210)[001]$ B'.B' and B.B GB (*left-hand side*) and for $\Sigma 5(310)[001]$ C and C₀ GB (*right-hand side*).

b. $\Sigma 5(310)[001]$ iron interlayers configurations : We present in Figure 13 the distribution of interlayer distances in the NM and FM configurations. Let us first comment on the results for the C stable structure. The main observation is that the profile is now highly asymmetrical between d_n and d_{-n} . More precisely, it is more rapidly damped on the right of the GB bilayer (for $n > 2.5$), with an extension limited to 2.5 Å, than on the left-hand-side where it extends up to 5 Å ($n < -4$, similarly to the (210) case). The corresponding profiles are $\{u-d-u-0-0-\dots\}$ on the right and $\{u-d-0-u-0-d-0-0-\dots\}$ on the left. No effect of magnetism is observed on this profile.

In the case of the C₀ structure, one recovers a quasi-symmetric profile, extending up to

6 Å on each side of the GB, as for (210) orientation. The main difference appears for Fe FM, in which case the interlayer which was initially centered has shifted for this structure without atom at $x=0$. In the same time, the amplitude of the oscillation is strongly reduced (by almost a factor 2).

c. Nickel interlayers configurations : Using the same notations as for iron, we present in Figure 14 the d_n/d_{bulk} distribution for the two nickel stable B'.B' and C GB, which are found symmetrical with no magnetism effect. The situation is similar for the two other B.B and C_0 structures.

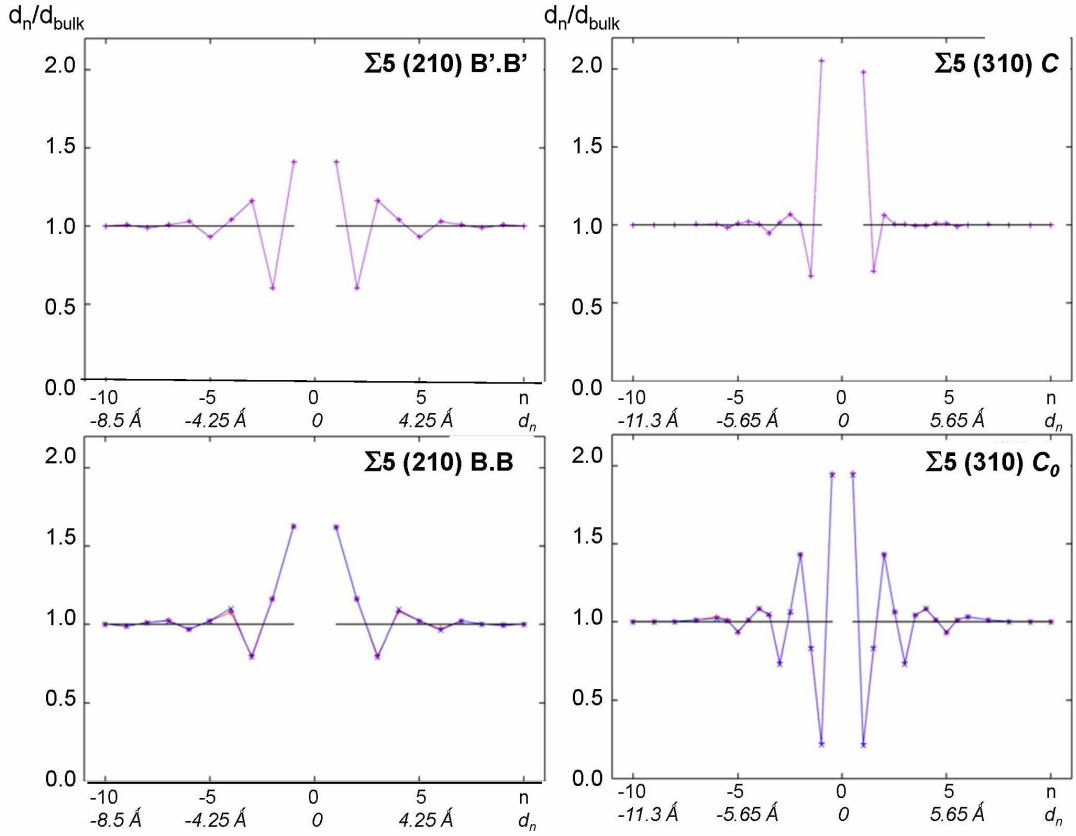


FIG. 14: Interlayer distance profiles d_n/d_{bulk} in both non magnetic (red line) and ferromagnetic (blue line) Ni for the $\Sigma 5(210)[001]$ B'.B' and B.B GB (*left-hand side*) and for $\Sigma 5(310)[001]$ C and C_0 GB (*right-hand side*). A single curve is shown for the B'.B' and C structures since NM and FM curves are undistinguishable

IV. LOCAL ANALYSIS

A. Energy and pressure mapping

In order to characterize GB on a deeper scale than the global formation energy, we now give local data which provide us a more detailed microscopic view. Let us first present maps of the excess energy and pressure *per* site for the different configurations, first for $\Sigma 5(210)[001]$ in iron (Figure 15) and nickel (Figure 16), then for $\Sigma 5(310)[001]$ in iron (Figure 17) and nickel (Figure 18). The excess energy *per* site is the extra energy compared to its bulk value so that it vanishes away from the GB. This mapping is important for a future study of segregation on the GB of Fe-Ni based alloy. Pressure is also a key parameter in segregation, since tensile (compressive) sites favours segregation of the element with the largest (lowest) atomic radius.

From a general point of view, let us note that a negative (resp. positive) pressure corresponds to a tensile (resp. compressive) site. Far from the GB, one therefore recovers the characteristics of the bulk with zero pressure and excess energy. This mapping shows that there exists strongly inequivalent sites in the GB region, with different properties, and that these are the sites presenting the highest excess energies which also undergo the largest pressure, and therefore the largest stress.

d. $\Sigma 5(210)[001]$ maps: Let us first comment on the maps obtained for iron in the non magnetic case. The most striking feature is that the stable B'.B' structure presents (as could have been guessed) sites with lower defect energies and pressure than the B.B one. Moreover, all these sites undergo a tensile stress in the B'.B' structure, consistently with the lateral expansion of the GB region previously found, whereas the few most stressed ones in the B.B structure are found in compression in spite of the global tensile stress, which would lead to drastically different behaviour in segregation problems. One can also note that the excess energy profile is more extended for B.B than for B'.B', which does not seem to be the case for the pressure profile. If one then consider the magnetic case, the most important effect is that magnetism drastically decreases the defect excess site energies (consistently with the previous results on the GB formation energy) and releases almost the whole stress, whatever its sign, in the GB region, for both B'.B' and B.B structures. Thus, even though one had not previously detected any noticeable changes in Figure 8 between NM and FM structures,

the corresponding energy or pressure maps of Figure 15 are found strongly different in both cases. This means that, even when magnetism does not change the microstructure of the GB, it significantly modifies its properties.

The maps obtained for nickel present similar trends, but with less amplitude. Namely, the stress undergone in the non magnetic case (and then the excess energies) is lower than for iron, but reversely it is less damped by the introduction of magnetism, so that GB presents a more important stress for iron than for nickel in the non magnetic case, but that the situation is reversed in the magnetic one.

e. $\Sigma 5(310)[001]$ maps: In that case, one recovers a global tensile behaviour for the stable C structure, a few less compressive sites than for the (210) still remaining in the non magnetic metastable C_0 one. The most striking feature is that the stress undergone by the system is drastically reduced whatever the magnetic state and the element with respect to the (210) structure. However similarly to the previous case, a few tensile sites remain in the stable C structure and compressive ones in the metastable C_0 one, the effect being more important for Fe than for Ni. Once again, this stress is almost completely released by magnetism for the stable C structure. The effect of magnetism is still more important for the C_0 structure for which, while changing the GB microstructure, it changes the sign of the stress which becomes slightly tensile instead of compressive.

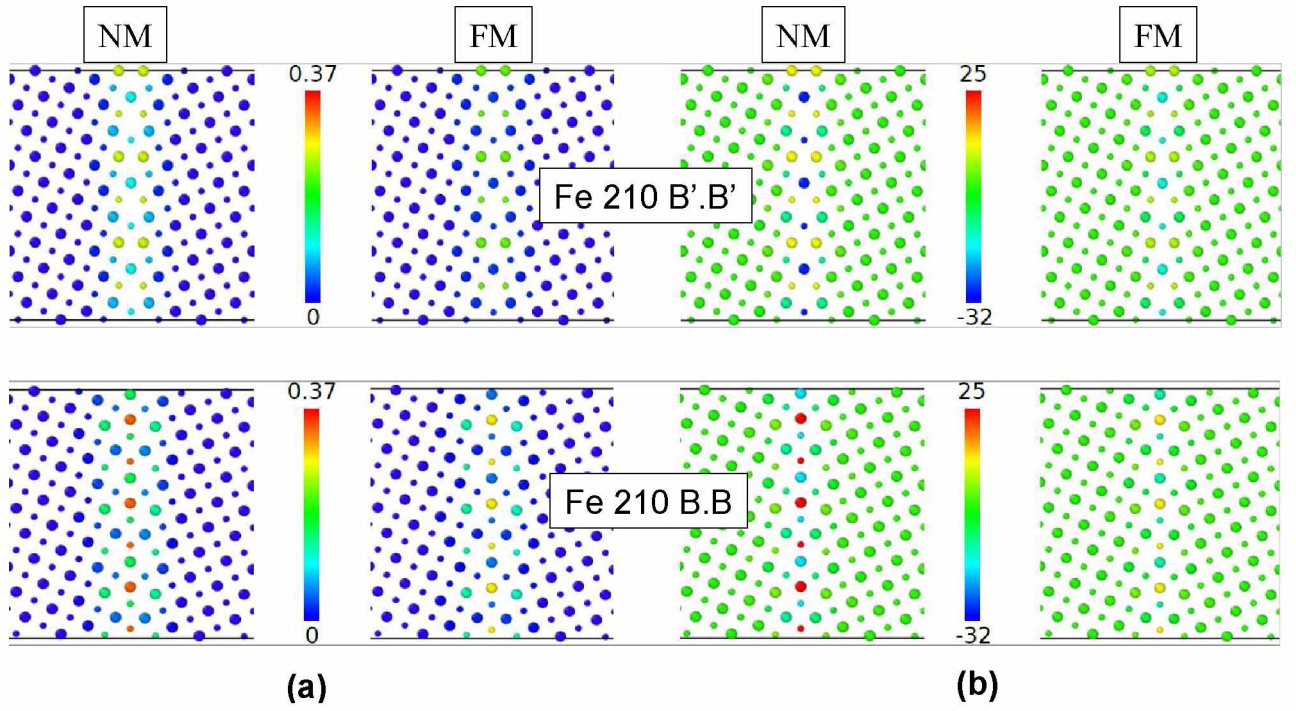


FIG. 15: Fe 210 mapping of (a) excess energies (eV) and (b) pressure (GPa) in NM and FM states.

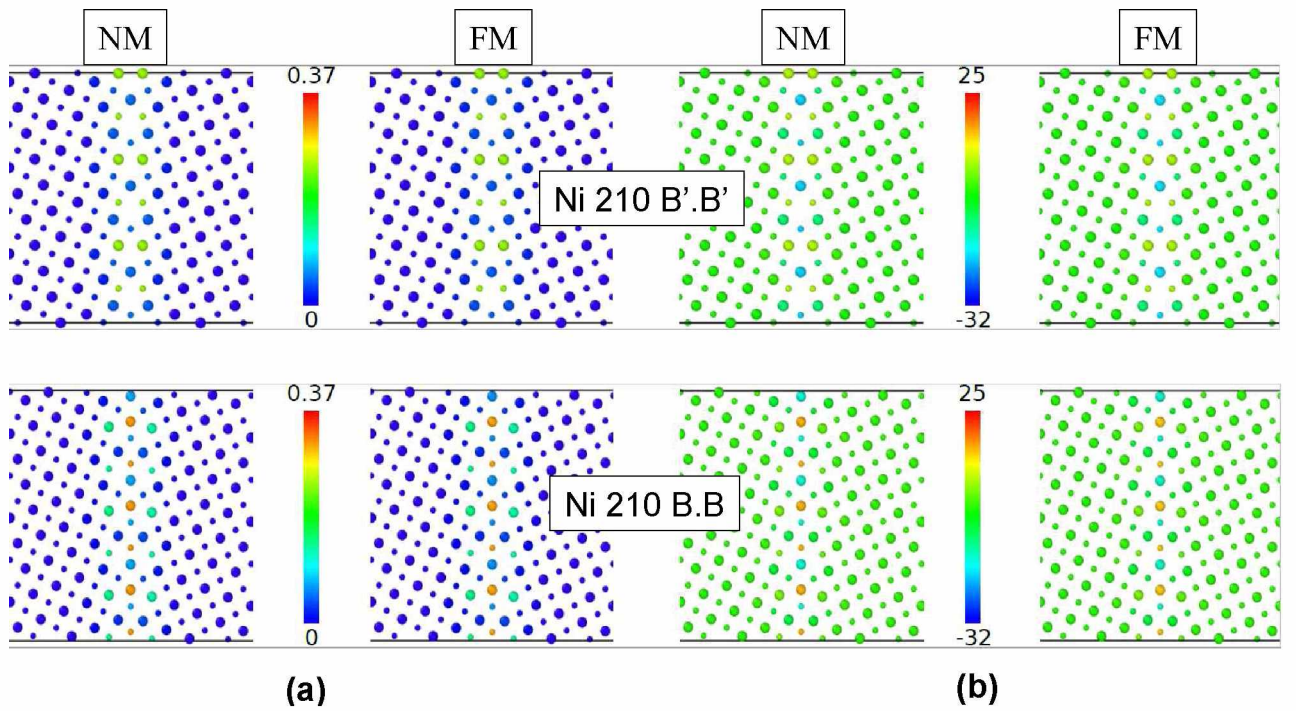


FIG. 16: Ni 210 mapping of (a) excess energies (eV) and (b) pressure (GPa) in NM and FM states.

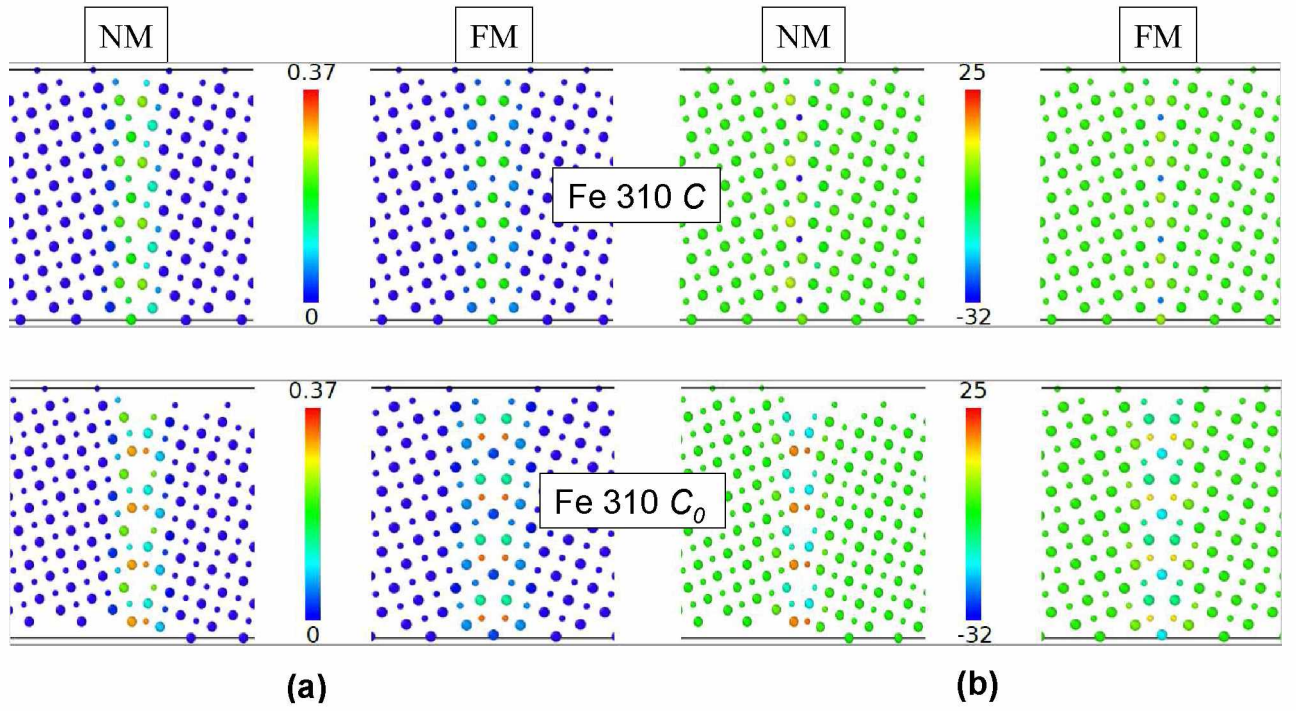


FIG. 17: Fe 310 mapping of (a) excess energies (eV) and (b) pressure (GPa) in NM and FM states.

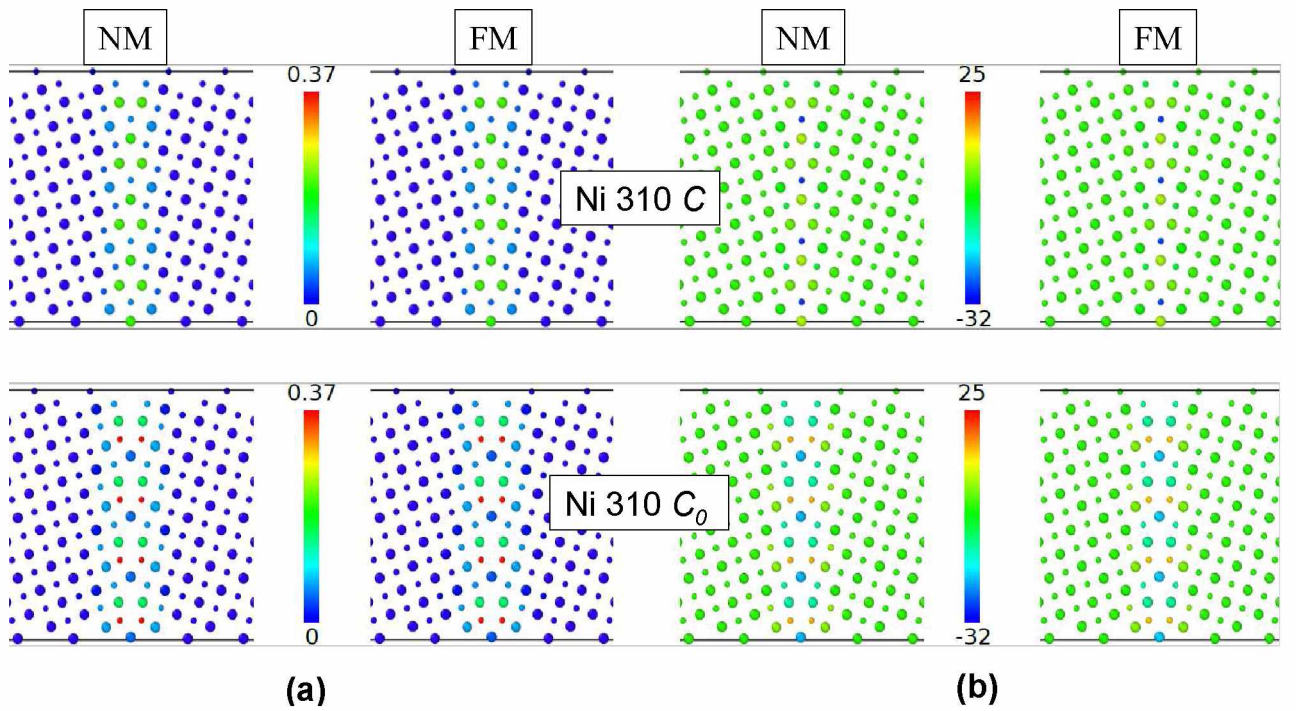


FIG. 18: Ni 310 mapping of (a) excess energies (eV) and (b) pressure (GPa) in NM and FM states.

B. Local reconstruction of the GB excess energy

The previous section has illustrated the inhomogeneity of the site energy maps in the GB region depending on the GB direction, on the microstructure and on the magnetic state. In order to determine the number of sites significantly perturbed by the presence of the defect in a boundary unit cell and which then contribute most to the GB formation energy, we can derive from the previous maps the number of sites N_{at} for which the local excess energy is larger than a given threshold E_{cut} , and the relative error ΔE made on the exact GB energy E_{GB} made by only considering their contribution E_{GB}^* : $\Delta E = E_{GB} - E_{GB}^*$.

More precisely, fixing a threshold $E_{cut}=0.001$ eV allows to reconstruct more than 95% of the total energy, with $N_{at} \simeq 16-18$ inequivalent sites for $\Sigma 5(210)[001]$ and $N_{at} \simeq 7-10$ sites for $\Sigma 5(310)[001]$. The perturbation due to the defect can then be considered as twice more extended in the former case than in the latter. If one now looks for the minimum number of sites necessary to reconstruct the energy, one finds that a higher threshold $E_{cut}=0.1$ eV is sufficient to reconstruct 70% of it and to recover semi-quantitatively all the energy trends, by just considering between 4 and 8 sites. From the variations of N_{at} and ΔE as a function of E_{cut} it is possible to characterize how the error on the energy depends on the number of sites considered. This is illustrated in the case of Fe NM (the results do not significantly depend on the nature of the element and on the magnetic state) in the Figure 19, in which we draw $\Delta E(E_{cut})$ as a function of $N_{at}(E_{cut})$. For each GB orientation, the corresponding points are found to gather on a same exponentially decreasing curve $\Delta E(N_{at})$. Using such a limited set of sites gives a useful way to characterize these GB at a lesser computational cost.

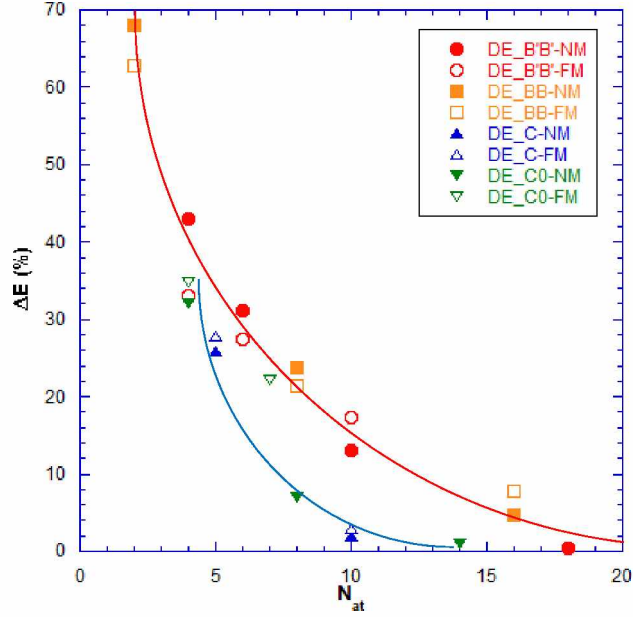


FIG. 19: Variation of the relative error ΔE made on the GB energy in non magnetic Fe by only considering the contribution of the N_{at} for which the local excess energy is larger than a given threshold E_{cut} , as a function of this number of sites N_{at} .

C. Local radial distance distribution function

Once identified the essential sites characteristic of the GB, *i.e.* responsible of the major part of the defect energy, it is possible to identify the origin of the respective stabilities of the different structures by just looking at the average coordinations $n(r)$ of this limited set of site. More precisely, $n(r)$ can be defined as the average number *per site* of all the numbers of neighbours included in a sphere of radius r around all these sites. This is illustrated in Figure 20 in which we plot the difference $dn(r)$ between this average coordination of atoms in the GB region and atoms in the bulk, for both the largest set ($E_{cut}=0.001$ eV, $N_{at} \simeq 15$ atoms) giving more than 95% of the energy, and the limited one ($E_{cut}=0.1$ eV, $N_{at} \simeq 5$ atoms) which gives about 70% but reproduce all the qualitative trends. The first observation is that the essential of the trends obtained for $E_{cut}=0.001$ eV are preserved by taking the limited set corresponding to $E_{cut}=0.1$ eV, which means that only a few atoms are sufficient to characterize the GB structures. As expected, one finds in each case a first positive contribution below the first neighbour distance since distances shorter than in the

bulk are generated by the GB. However, this contribution is found similar in all cases, in particular one recovers that relaxation suppresses the too short distances initially present in the C_0 structure which then presents a similar short distance coordination as C in spite of its larger compactness. Then, as can be seen, the analysis is clear for $\Sigma 5(210)[001]$, since the stablest B'.B' structure presents a radial distribution function much more closer to that of perfect bulk than that of B.B in the distance region between first (r_0) and second (r_c^1) neighbours, which prevails in the TB-SMA potential. This is less clear for $\Sigma 5(310)[001]$ although this limited set of sites well reproduces the stability trend in that case also.

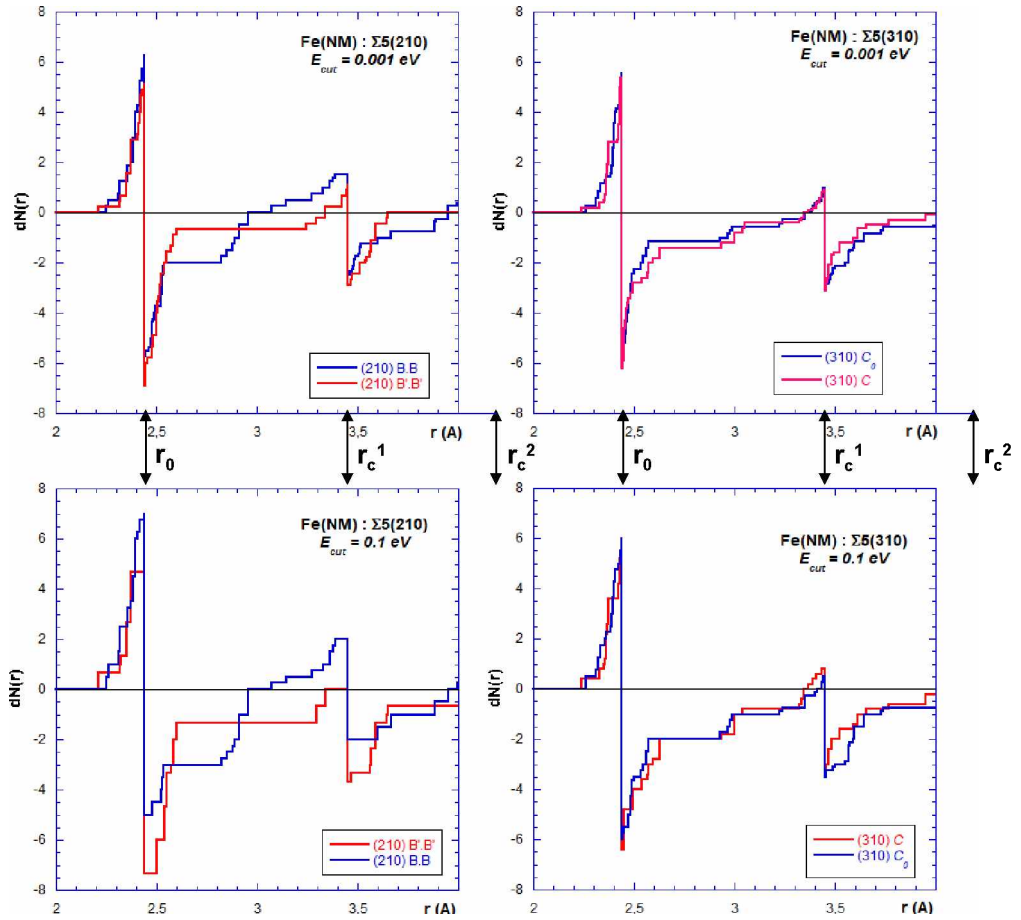


FIG. 20: Variation of the average coordination $n(r)$ in the grain boundary region with respect to bulk for non magnetic iron, calculated on the limited sets of sites which contribute to more than 95% ($E_{cut}=0.001$ eV, upper side) and 70% ($E_{cut}=0.1$ eV, lower side) of the total GB formation energy. The first (r_0), second (r_c^1) and third (r_c^2) neighbours distances in the bulk are indicated.

V. CONCLUSION

We have presented here a theoretical study of the effect of magnetism on the relative stabilities of the main microstructures which can exist in the most common $\Sigma 5$ (210) and (310) [001] tilt boundaries in fcc Ni and Fe. To this aim we have developed a new interatomic potential in the framework of the second moment approximation of the Tight-Binding scheme which accounts for magnetic effects. Then we performed quenched molecular dynamics simulations grounded on this potential to compare the respective stabilities and microstructures of the different GB. Similar results are found for Fe and Ni, although magnetic effects are found more important in the former case for which it significantly lowers the excess GB energy. In addition, it has been shown that magnetism strongly reduces the stress in the GB region and that it can modify the relaxation profile. For a few GB orientations, magnetism can even change the GB microstructure. But the main result remains that, even when magnetism does change the GB microstructure, it drastically modifies its energetic and stress properties. Finally a local analysis has been proposed which allows to classify the relative stabilities of the different structures in terms of only a few given atomic sites.

-
- [1] FJ Humphreys and M Hatherly. Grain growth following recrystallization. *Recrystallization and related annealing phenomena*, 1:281325, 1995.
 - [2] Gunter Gottstein and Lasar S Shvindlerman. *Grain boundary migration in metals: thermodynamics, kinetics, applications*. CRC press, 2009.
 - [3] Adrian P Sutton, Robert W Balluffi, and AP Sutton. Interfaces in crystalline materials. 1995.
 - [4] Moneesh Upmanyu, Gregory N Hassold, Andrei Kazaryan, Elizabeth A Holm, Yunzhi Wang, B Patton, and David J Srolovitz. Boundary mobility and energy anisotropy effects on microstructural evolution during grain growth. *Interface Science*, 10(2-3):201–216, 2002.
 - [5] D Wolf and S Phillpot. Role of the densest lattice planes in the stability of crystalline interfaces: A computer simulation study. *Materials Science and Engineering: A*, 107:3–14, 1989.
 - [6] D Wolf. Structure and energy of general grain boundaries in bcc metals. *Journal of applied physics*, 69(1):185–196, 1991.
 - [7] David M Saylor, Bassem S El Dasher, Anthony D Rollett, and Gregory S Rohrer. Distribution

- of grain boundaries in aluminum as a function of five macroscopic parameters. *Acta Materialia*, 52(12):3649–3655, 2004.
- [8] William T Read and W Shockley. Dislocation models of crystal grain boundaries. *Physical review*, 78(3):275, 1950.
- [9] Elizabeth A. Holm, David L Olmsted, and Stephen M Foiles. Comparing grain boundary energies in face-centered cubic metals: Al, au, cu and ni. 2010.
- [10] D Yesiltepe and TA Arias. Atomic-level physics of grain boundaries in bcc molybdenum. *Physical Review B*, 64(17):174101, 2001.
- [11] Pavel Lejček and Siegfried Hofmann. Thermodynamics and structural aspects of grain boundary segregation. *Critical Reviews in Solid State and Material Sciences*, 20(1):1–85, 1995.
- [12] Sutatch Ratanaphan, David L Olmsted, Vasily V Bulatov, Elizabeth A Holm, Anthony D Rollett, and Gregory S Rohrer. Grain boundary energies in body-centered cubic metals. *Acta Materialia*, 88:346–354, 2015.
- [13] F Berthier, B Legrand, and G Tréglia. New structures and atomistic analysis of the polymorphism for the sigma 5 (210)[001] tilt boundary. *Interface Science*, 8(1):55–69, 2000.
- [14] K Hampel, DD Vvedensky, and S Crampin. Magnetic structure near (310) tilt boundaries in iron. *Physical Review B*, 47(8):4810, 1993.
- [15] WT Geng, Arthur J Freeman, R Wu, CB Geller, and JE Raynolds. Embrittling and strengthening effects of hydrogen, boron, and phosphorus on a σ 5 nickel grain boundary. *Physical Review B*, 60(10):7149, 1999.
- [16] Ivan Bleskov, Tilmann Hickel, Jörg Neugebauer, and Andrei Ruban. Impact of local magnetism on stacking fault energies: A first-principles investigation for fcc iron. *Physical Review B*, 93(21):214115, 2016.
- [17] Somesh Kr Bhattacharya, Shingo Tanaka, Yoshinori Shiihara, and Masanori Kohyama. Ab initio study of symmetrical tilt grain boundaries in bcc fe: structural units, magnetic moments, interfacial bonding, local energy and local stress. *Journal of Physics: Condensed Matter*, 25(13):135004, 2013.
- [18] PD Bristowe and AG Crocker. The structure of high-angle (001) csl twist boundaries in fcc metals. *Philosophical Magazine A*, 38(5):487–502, 1978.
- [19] Gui Jin Wang, AP Sutton, and V Vitek. A computer simulation study of $\{001\}$ and $\{111\}$ tilt boundaries: the multiplicity of structures. *Acta Metallurgica*, 32(7):1093–1104, 1984.

- [20] D Scheiber, R Pippin, P Puschnig, and L Romaner. Ab initio search for cohesion-enhancing impurity elements at grain boundaries in molybdenum and tungsten. *Modelling and Simulation in Materials Science and Engineering*, 24(8):085009, 2016.
- [21] Xuebang Wu, Yu-Wei You, Xiang-Shan Kong, Jun-Ling Chen, G-N Luo, Guang-Hong Lu, CS Liu, and Zhiguang Wang. First-principles determination of grain boundary strengthening in tungsten: dependence on grain boundary structure and metallic radius of solute. *Acta Materialia*, 120:315–326, 2016.
- [22] V. Rosato, M. Guillope, and B. Legrand. Thermodynamical and structural properties of f.c.c. transition metals using a simple tight-binding model. *Philosophical Magazine A*, 59(2):321–336, 1989.
- [23] D Spanjaard and MC Desjonquères. Comment on” universal features of bonding in metals”. *Physical Review B*, 30(8):4822, 1984.
- [24] I. A. Abrikosov, A. E. Kissavos, F. Liot, B. Alling, S. I. Simak, O. Peil, and A. V. Ruban. Competition between magnetic structures in the fe rich fcc feni alloys. *Phys. Rev. B*, 76:014434, Jul 2007.
- [25] Preetma Soin, Andrew P Horsfield, and D Nguyen-Manh. Efficient self-consistency for magnetic tight binding. *Computer Physics Communications*, 182(6):1350–1360, 2011.
- [26] Ralf Drautz and DG Pettifor. Valence-dependent analytic bond-order potential for magnetic transition metals. *Physical Review B*, 84(21):214114, 2011.
- [27] Michael E Ford, Ralf Drautz, Thomas Hammerschmidt, and DG Pettifor. Convergence of an analytic bond-order potential for collinear magnetism in fe. *Modelling and Simulation in Materials Science and Engineering*, 22(3):034005, 2014.
- [28] M Sansa, A Dhouib, F Ribeiro, B Legrand, G Trégliã, and C Goyhenex. Tight-binding modelling of ferromagnetic metals and alloys. *Modelling and Simulation in Materials Science and Engineering*, 25(8):084004, 2017.
- [29] Graeme J Ackland. Two-band second moment model for transition metals and alloys. *Journal of nuclear materials*, 351(1-3):20–27, 2006.
- [30] Jonathan J Bean and Keith P McKenna. Origin of differences in the excess volume of copper and nickel grain boundaries. *Acta Materialia*, 110:246–257, 2016.
- [31] James R Rice and Robb Thomson. Ductile versus brittle behaviour of crystals. *The Philosophical Magazine: A Journal of Theoretical Experimental and Applied Physics*, 29(1):73–97,

1974.

- [32] Alan F.Liu. *Mechanics and Mechanisms of Fracture: An Introduction*. ASM International, 2005.
- [33] David L Olmsted, Stephen M Foiles, and Elizabeth A Holm. Survey of computed grain boundary properties in face-centered cubic metals: I. grain boundary energy. *Acta Materialia*, 57(13):3694–3703, 2009.